Polymer Chemistry

ROYAL SOCIETY OF CHEMISTRY

PAPER

View Article Online
View Journal | View Issue

Open Access Article. Published on 10 Mart 2023. Downloaded on 9.09.2024 20:37:54.
This article is licensed under a Creative Commons Attribution-NonCommercial 3.0 Unported Licence.

Check for updates

Cite this: *Polym. Chem.*, 2023, **14**, 1526

Cosolvent effects on the structure and thermoresponse of a polymer brush: PNIPAM in DMSO–water mixtures†

Hayden Robertson,[a] Andrew R. J. Nelson,[b] Stuart W. Prescott,[c] Grant B. Webber[a] and Erica J. Wanless *[a]

Cosolvents play an integral role in polymer solubility, with myriad applications in drug delivery and energy storage. In particular, dimethyl sulfoxide (DMSO) has received substantial attention to date due to its cryoprotective properties and interesting nonideal mixing behaviour. Here, for the first time, we probe the fundamentals of DMSO–water solvent structuring using a thermoresponsive poly(*N*-isopropoylacrylamide) (PNIPAM) brush as an exemplar. Spectroscopic ellipsometry and neutron reflectometry were employed to monitor changes in brush swelling and conformation as a function of temperature and solvent composition, whereby changes in solvent structure can be deduced. Importantly, unlike free polymer, grafted polymers permit measurements across the entire solvent composition space, including 'poor' solvent conditions, permitting the characterisation of polymers in complex media for future technologies. In the water-rich regime, the prevalent hydrogen-bond network resulted in the PNIPAM brush exhibiting a lower critical solution temperature (LCST) up to DMSO mole fractions of 0.10 (x_D = 0.10), which decreased with increasing x_D; DMSO is a chaotropic cosolvent. This region was adjacent to a cononsolvency region. Interestingly, reentrant swelling was observed for above approximately x_D = 0.2. In DMSO-rich regimes, non-site-specific dipole–dipole interactions resulted in the PNIPAM brush exhibiting an uppercritical solution temperature (UCST), whereby the periphery of the swollen brush was more diffuse than at low x_D. At all temperatures, pure DMSO is a good solvent for PNIPAM and no thermoresponse was observed. Herein we demonstrate how the structure and swelling of a polymer brush film can be modulated by tuning solvent composition by mixing two 'good' solvents.

Received 28th November 2022,
Accepted 12th February 2023

DOI: 10.1039/d2py01487d

rsc.li/polymers

1 Introduction

Stimulus-responsive polymers respond to changes in the surrounding environment by altering their conformation.[1–4] When densely grafted to a surface, these polymers form a 'brush' with switchable interfacial and physicochemical properties; establishing a basis for smart coatings,[1,5–7] with myriad applications ranging from controlled drug delivery to rheology modification.[8,9] One subset of stimulus-responsive polymers is thermoresponsive polymers, such as poly(*N*-isopropylacrylamide) (PNIPAM) or polymers from the poly(oligo (ethylene glycol methyl ether methacrylate) (POEGMA) family, which undergo a thermotransition at a critical temperature.[4,10] Classically, a lower critical solution temperature (LCST) describes a soluble to insoluble transition, where polymer solubility decreases with increasing temperature in solution. Additionally, an upper critical solution temperature delineates a collapsed to swollen transition, where polymer solubility increases with temperature.

Dimethyl sulfoxide (DMSO) is a common polyfunctional organic solvent with a prevalence in biotechnology.[11,12] Specifically, DMSO and water–DMSO mixtures have received great attention for their radioprotective and cryoprotective properties, high membrane penetration, and protein denaturing capabilities.[13–17] Binary mixtures of DMSO and water have been shown to exhibit nonideal mixing behaviour,[9,12,18–20] manifesting as unexpected and complex variations in thermophysical properties such as the freezing point,[21] density,[22] viscosity,[22–24] dielectic relaxation time,[25] and surface tension.[23] Deviations from ideality have been attributed to the strong hydrogen-bond formed between DMSO and water, leading to the increase in the polarisation of DMSO and water

[a]College of Science, Engineering and Environment, University of Newcastle, Callaghan, Australia. E-mail: erica.wanless@newcastle.edu.au
[b]ANSTO, Locked Bag 2001, Kirrawee DC, NSW 2232, Australia
[c]School of Chemical Engineering, UNSW, Sydney, NSW 2052, Australia

† Electronic supplementary information (ESI) available. See DOI: https://doi.org/10.1039/d2py01487d. Data and notebooks required to reproduce analysis are readily available on Zenodo at https://doi.org/10.5281/zenodo.7359324.

This journal is © The Royal Society of Chemistry 2023

Open Access Article. Published on 10 Mart 2023. Downloaded on 9.09.2024 20:37:54.
This article is licensed under a Creative Commons Attribution-NonCommercial 3.0 Unported Licence.

molecules.[12,20,26] Moreover, molecular dynamics simulations by Zhang *et al.* have shown non-monotonic trends in water reorientation dynamics with increasing DMSO content, deviating from ideality and aligning with viscosity trends.[20] In water-rich regimes, Zhang *et al.* note retardation of the water reorientation due to steric effects imparted by the DMSO co-solvent. However, in DMSO-rich regimes, the authors describe faster water reorientations; the increased hydrophobic environment breaks the hydrogen-bond network into smaller aggregates.

Despite DMSO being highly self-associative,[12,27,28] in binary mixtures with water, DMSO–water intermolecular interactions are stronger and more energetically favourable than DMSO–DMSO and water–water self-interactions.[13,20,28] In water-rich regimes (*i.e.*, low DMSO mole fraction, x_D), neutron diffraction,[26,29,30] dielectric and FTIR spectroscopy,[19,28] and molecular dynamics studies[14,20,24] suggest the predominance of 1DMSO : $2H_2O$ clusters as well as some 1DMSO : $3H_2O$ aggregates.[21,31,32] Initially, at very low x_D, water–water interactions are statistically prevalent as the liquid still assumes the structural and thermodynamic properties of pure water.[13] As x_D increases, water–water hydrogen-bonds rupture, decreasing the length of water–water hydrogen-bond chains. This substantially reduces the total number of water–water hydrogen-bonds as water begins to interact more strongly with DMSO molecules;[14] however, the short-range water structure is still maintained.[28] At the stoichiometric equivalence point (1DMSO : $2H_2O$; x_D = 0.33), a saturation of DMSO hydrogen-bonds occurs, which has been shown to be the DMSO–water eutectic point.[12,19,28] Catalán *et al.* performed UV-Vis spectroscopy measurements to characterise the acidity, basicity and polarity of the binary mixtures, suggesting that their behaviour is governed by 1DMSO : $1H_2O$ clusters around concentrations of equal DMSO and water content.[23] In DMSO-rich regimes, the complete hydration of DMSO molecules is impossible due to insufficient water molecules; the behaviour is dominated by DMSO self-interaction.[28] Previous investigations have shown that both 2DMSO : $1H_2O$ and 3DMSO : $1H_2O$ aggregates prevail,[19,20,28,33] whereby water inserts itself inside the cluster, being shielded from its surroundings.[13,34]

The thermoresponsive behaviour of PNIPAM can be tuned as a function of the bulk solvent quality and electrolyte strength and identity.[34–37] In pure water, PNIPAM is known to exhibit an LCST at approximately 32.5 °C; however, as DMSO is a 'good' solvent for PNIPAM the thermoresponse is substantially suppressed in such a way that no thermotransition is observed across the examined temperature ranges, as the dispersed polymer never self-associates.[11,38] Curiously, in solvent mixtures of DMSO and water, PNIPAM exhibits both LCST and UCST behaviour. Investigations into the thermotransition and solvation of free PNIPAM and PNIPAM gels have shown that LCST behaviour is observed at x_D = 0.06, where small additions of a 'good' solvent result in a decrease in the LCST.[11,38–40] At x_D = 0.70, a UCST has been observed for ungrafted PNIPAM, which decreases in temperature with increasing x_D.[11,38] The large cononsolvency region between the LCST and UCST (*i.e.*, between x_D = 0.06 and 0.70) has been attributed to preferential DMSO–water interactions relative to DMSO–PNIPAM and water–PNIPAM interactions at intermediate x_D.[38] The presence of both types of thermotransition (LCST and UCST) is rare for a polymer in a binary solvent.

The behaviour of PNIPAM brushes in non-aqueous solvents has received little attention to date.[41] To the authors' knowledge, there have been no reports on the behaviour and structure of PNIPAM brushes in binary DMSO–water solvent mixtures. Polymer brushes on planar substrates are particularly valuable as they have the potential to provide information on both polymer solvation and conformation agnostic of solvent quality, *i.e.*, both well-solvated and poorly-solvated environments. This is unlike the colloidal instability observed with PNIPAM gels[40,42] and microgels,[43] PNIPAM brushes on silica particles,[44] and linear free PNIPAM.[34] Herein we investigate the modulation of the PNIPAM LCST and brush solvation as a function of DMSO mole fraction (up to x_D = 0.50) with spectroscopic ellipsometry over a broad temperature range from 12.5 °C to 55 °C. Neutron reflectometry (NR) was employed to monitor the detailed brush conformation as a function of both x_D and temperature. NR measurements were conducted across the entire range of DMSO mole fraction in water (x_D = 0 to x_D = 1), covering both the LCST and UCST behaviours; unveiling distinctly different solvent-dependent structures.

2 Experimental

2.1 Materials

Native oxide silicon wafers used for spectroscopic ellipsometry (0.675 mm thick) and neutron reflectometry (∅ 100 mm; 10 mm thick) measurements were purchased from Silicon Valley Microelectronics (USA) and El-Cat Inc.(USA), respectively. Sodium hydroxide (NaOH) used for surface cleaning was purchased from Chem-Supply. Surface functionalisation reagents, 2-bromoisobutanoate bromide (BIBB, >99%), (3-aminopropyl) triethoxysilane (APTES, >99%) and triethylamine (TEA, 99%), were purchased from Sigma-Aldrich and used as received. Tetrahydrofuran (THF, >99%) was purchased from RCI Labscan Ltd and dried over 4 Å molecular sieves prior to use. Methanol and ethanol were purchased from Thermofisher Scientific and were used as received as a polymerisation cosolvent and to clean surfaces, respectively. Copper bromide ($CuBr_2$, 99.999%), (+)-sodium L-ascorbate (>98%) and 1,1,4,7,10,10-hexamethyltriethylenetetramine (HMTETA, 97%) were purchased from Sigma-Aldrich and used as received as polymerisation reagents. *N*-Isopropyl-acrylamide (NIPAM) monomer was purchased from Sigma-Aldrich and purified by recrystallisation from hexane (Sigma-Aldrich) prior to use. Dimethyl sulfoxide (DMSO, anhydrous, ≥99.9%) and deuterated dimethyl sulfoxide (d-DMSO, anhydrous, 99.9 atom % D) were purchased from Sigma-Aldrich and used as received. MilliQ water (Merck Millipore, 18.2 MΩ cm at 25 °C) was used throughout, excluding neutron reflectometry experiments which used D_2O (Sigma-Aldrich). All glassware was thoroughly

Open Access Article. Published on 10 Mart 2023. Downloaded on 9.09.2024 20:37:54.
This article is licensed under a Creative Commons Attribution-NonCommercial 3.0 Unported Licence.

washed with MilliQ water and ethanol prior to washing in a 10% HNO_3 acid bath for at least 24 hours.

2.2 PNIPAM brush synthesis

Silicon wafers for spectroscopic ellipsometry and neutron reflectometry were functionalised according to our previously reported method.[3,45,46] PNIPAM brushes were synthesised adhering to an established protocol, which was upscaled for the 100 mm silicon blocks used for neutron reflectometry experiments.[3] To achieve appropriate polymerisation kinetics, a 4 : 1 v/v methanol/water solvent ratio was used in conjunction with a monomer/catalyst/ligand/reducing agent molar ratio of 900/1/10/10 with NIPAM/$CuBr_2$/HMTETA/sodium ascorbate. A summary of the dry thickness for each PNIPAM brush sample is presented in Table 1.

2.3 Spectroscopic ellipsometry

Spectroscopic ellipsometry measurements were conducted on an Accurion EP4 variable angle spectroscopic imaging ellipsometer.[2,3] Surface mapping of the dry brush was performed at a single wavelength (658 nm) across four equally spaced angles of incidence from 40 to 70°. *In situ* measurements were conducted on a single brush sample in a solid–liquid cell at an angle of incidence of 65° across 12 equidistant wavelengths from 400 to 910 nm. All temperature ramps were performed with increasing temperature, and the sequence of experimental conditions was in the order of increasing DMSO mole fraction. Intermittent 'water checks' were performed to confirm the ongoing expected baseline brush behaviour.

The analysis of ellipsometry data was performed using the *refellips* analysis package.[47] A four-component model, analogous to our neutron reflectometry approach, was used to model and fit all ellipsometry data. The model consisted of four slabs that describe each component's optical properties, thickness, roughness and solvent volume fraction. From 'fronting' to 'backing', the structure for the *in situ* measurements was water, polymer, silica and silicon, respectively. For dry measurements, the water component was replaced with air. All data and code required to reproduce the analysis presented here are readily available on Zenodo.[48]

Ellipsometry results are represented as a swelling ratio (SR; quotient of solvated and dry brush thicknesses) to allow for normalisation across different polymer brush samples. It should be noted that due to the intrinsic physical properties of PNIPAM and DMSO, not all solvent compositions could be explored with ellipsometry. Namely, there is insufficient contrast between the refractive indices of PNIPAM and solvent at high x_D for reliable measurements.

Table 1 Summary of PNIPAM dry brush thickness[a] for each brush investigated in this study

In situ measurement	Ellipsometrically determined dry brush thickness (Å)	NR determined dry brush thickness (Å)
Ellipsometry	340.1 ± 0.9	—
NR	244.2 ± 4.1	265.3 ± 0.3

[a] Associated uncertainties for each technique are determined *via* different sources. For ellipsometry measurements, uncertainties are taken as the standard deviation from 32 distinct measurements across the surface. For neutron reflectometry measurements, uncertainties are derived from PT-MCMC sampling.

2.4 Neutron reflectometry

Specular neutron reflectivity measurements were performed on the *PLATYPUS* time-of-flight neutron reflectometer at the OPAL 20 MW nuclear reactor at the Australian Centre for Neutron Scattering (ANSTO, Lucas Heights, Australia).[49] Dry measurements were collected over a Q-range of 0.009 to 0.31 $Å^{-1}$ at angles of incidence of 0.6° and 3.0°. For all *in situ* measurements, reflectivity was collected over a Q-range of 0.009 to 0.07 $Å^{-1}$ with a constant dQ/Q of 8.8% at an angle of incidence of 0.8°. We have previously characterised the behaviour and structure of PNIPAM brushes with NR across a broad extent of conditions and wider Q-range.[3,46,50,51] A larger Q-range was not possible in this study due to access restraints. A comparison of optimised models, scattering length density (SLD) profiles and volume fraction (VF) profiles against identical reflectivity measurements of small and large Q-ranges is presented in the ESI, Fig. S3.2.† As per previous experiments, reflectivity was measured in an upward-reflecting geometry, with samples placed in temperature-controlled solid–liquid cells.[2,3,50,51] All temperature ramps were performed with increasing temperature, aligning with ellipsometry experiments. Prior to exposing the brush to new solvent compositions, the cell was flushed with D_2O. Data were collected for at least 15 minutes to allow for adequate statistics.

2.5 Analysis of neutron reflectometry data

All NR data obtained were modelled and optimised using *refnx*.[50,52] The employed model for all analyses was informed by our previous studies,[2,3,51] and consisted of two main components: a series of uniform layers (*i.e.*, slabs) and a piecewise cubic Hermite interpolating polynomial. From 'fronting' to 'backing', the model commenced with three slabs which describe the silicon phase, the native oxide layer, and the dense interior polymer layer, respectively. The model then contained a free-form spline delineating the diffuse periphery of the polymer brush, which is subsequently capped by a solvent slab. For modelling the dry brush, the free-form spline was not required and the solvent slab was replaced with air. The SLD of the silicon and silica slabs was fixed to literature values of 2.07×10^{-6} $Å^{-2}$ and 3.47×10^{-6} $Å^{-2}$, respectively,[50] and the solvent VF of the silica slab was permitted to vary between 0 and 0.4, inclusive, due to the known porosity of silica.[2,51] As per previous investigations, the SLD of the interior polymer slab proximal to the interface was set to be 0.78×10^{-6} $Å^{-2}$, and was permitted to vary over a narrow range to account for isotopic substitution of the amide proton on the NIPAM monomer.[3,51] The piecewise interpolating polynomial consisted of 4 knots, where the VF and distance between each knot were permitted to vary and the adsorbed interfacial

 This journal is © The Royal Society of Chemistry 2023

Open Access Article. Published on 10 Mart 2023. Downloaded on 9.09.2024 20:37:54.
This article is licensed under a Creative Commons Attribution-NonCommercial 3.0 Unported Licence.

volume was constrained by the dry brush thickness (Table 1). Monotonicity in the polymer VF profiles was enforced across all conditions.

From the above-established model, the polymer VF profile, $\phi(z)$, was calculated *via* the theoretical SLD profile ($\rho_N(z)$):

$$\rho_N(z) = \phi(z)\rho_{N,Polymer} + (1 - \phi(z))\rho_{N,Solvent} \quad (1)$$

where z is the orthogonal distance from the substrate and $\rho_{N,Polymer}$ and $\rho_{N,Solvent}$ represent the SLD of the polymer and solvent, respectively. The reflectivity profile was then calculated using the Abeles matrix formalisation and compared to the measured reflectivity profile. The model and measured data were initially optimised using differential evolution, followed by parallel tempered Markov chain Monte Carlo (PT-MCMC) sampling of the posterior distribution. All optimised fits and VF profiles presented in this study correspond to the median of the posterior distribution function, extracted from a very narrow distribution of PT-MCMC samples. Note that the distribution of SLD and VF profiles (Fig. S3.3†) around the structure corresponding to the thermotransition temperature is slightly broader relative to other temperatures due to the reduced Q-range. Finally, the average brush thickness at a given condition was extracted from the VF profile as twice the normalised first moment (eqn (2)). Further details regarding this modelling procedure are illustrated by Gresham *et al.*,[50] with all data and code required to reproduce the analyses in this study available on the Zenodo repository.[48]

$$L_{1st} = 2\frac{\int_0^\infty z \cdot \phi(z)\,dz}{\delta_{dry}} \quad (2)$$

3 Results and discussion

Modulation of the thermoresponse and swelling of a PNIPAM brush were monitored using spectroscopic ellipsometry and neutron reflectometry (NR) as a function of DMSO mole fraction (x_D). LCST-type behaviour was confirmed with ellipsometry, while NR was employed to investigate the changes in polymer conformation across the entire range of x_D as a function of temperature. For spectroscopic ellipsometry measurements, only compositions up to x_D = 0.50 were investigated due to insufficient contrast between the solvent and polymer; NR was employed to probe these DMSO-rich regimes.

3.1 Brush behaviour in a water-rich solvent

Fig. 1 presents the ellipsometrically determined brush thickness and resultant swelling ratio as a function of both x_D and temperature. Ellipsometry data is divided into two regimes exhibiting different brush responses as a function of temperature: LCST region for $x_D \leq 0.1$ (●, Fig. 1) and cononsolvency region for $0.1 < x_D \leq 0.5$ (×, Fig. 1). We start by examining the LCST regime.

In the presence of pure water (x_D = 0), PNIPAM undergoes the expected LCST thermotransition at approximately 32 °C;

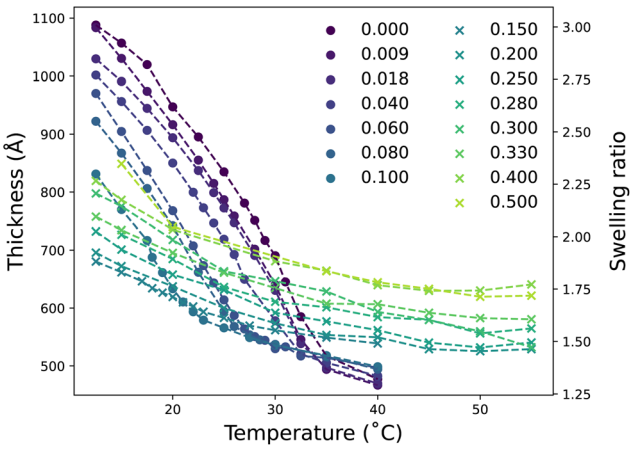

Fig. 1 Ellipsometry determined thickness and swelling ratio of a PNIPAM brush as a function of x_D and temperature. Circle symbols (●) denote solvent compositions where a clear thermotransition is observed; crosses (×) denote compositions with a severely suppressed thermotransition.

brush thickness decreases as a function of temperature.[3,45,53–55] At temperatures below the LCST the influence of temperature on brush thickness is greater than above the LCST. Small additions of DMSO to the PNIPAM–water mixture are known to influence the thermoresponse of ungrafted PNIPAM drastically.[36] Here we observe that upon changing the solvent composition to include a small mole fraction of DMSO (x_D = 0.009) the thermotransition is shifted to a lower temperature, which is accompanied by a decreased brush thickness relative to the absence of DMSO. This effect persists up to x_D = 0.10, with the thermotransition and brush thickness at a given temperature decreasing as x_D increases. Fig. S2.1† presents the accompanying derived LCST values of PNIPAM in these solvent compositions, illustrating a non-linear decrease in thermotransition with increasing x_D. The non-linear dependence of PNIPAM brush LCST with increasing x_D is in concordance with previous investigations demonstrating the nonideal behaviour of DMSO–water solutions.[21–23] The underlying mechanics behind this decrease in LCST with increasing x_D will be discussed later in §3.2.1.

At concentrations at and above x_D = 0.15, the thermoresponse is suppressed over the explored temperature range. In this second region, the brush has a smaller thermoresponse with reduced changes in brush thickness observed with increasing temperature. Here no clear inflection is present, which would be indicative of LCST-type behaviour. Interestingly, the brush thickness at all temperatures is observed to increase with x_D; providing evidence for reentrant swelling. Furthermore, the brush does not fully collapse as observed in x_D = 0. The slight increase in brush thickness from x_D = 0.15 to x_D = 0.50 aligns with previous swelling measurements on PNIPAM gels in binary solvents of DMSO and water from Mukae *et al.*, which illustrate a broad reentrant swelling after an initial, abrupt collapse up to x_D = 0.10.[40] Fig. S2.2† demonstrates that at a fixed temperature of 15 °C, the change

Open Access Article. Published on 10 Mart 2023. Downloaded on 9.09.2024 20:37:54.
This article is licensed under a Creative Commons Attribution-NonCommercial 3.0 Unported Licence.

in brush thickness is non-monotonic in nature with a minimum at x_D = 0.15. This aligns with the dual behaviour evident in Fig. 1, whereby a clear thermotransition is only observed up to approximately x_D = 0.10 followed by broad reentrant behaviour. Analogous behaviour is also observed for the brush at 25 °C and 30 °C, where the minimum is shifted to lower x_D. However, at 40 °C the brush thickness is seen to undergo an almost monotonic increase with increasing x_D.

3.2 Internal structure of the brush

To probe the subtle changes in the structure of a PNIPAM brush, neutron reflectometry (NR) was employed where measurements were performed as a function of temperature across the entire solvent composition range. The NR-derived polymer brush volume fraction (VF) profiles have a 'proximal layer' adjacent to the substrate, an 'inner region', and a 'diffuse tail' at the periphery of the brush.[3,50] We also denote the 'bottom-up' desolvation and collapse as an increasing inner region with a low polymer VF tail.[10,46,56] Herein, the description of the polymer VF profiles will be split into three solvent composition regimes of increasing DMSO mole fraction: a region of LCST-type behaviour (low DMSO content), a cononsolvency region (intermediate DMSO content), and a DMSO-rich region. We commence by discussing the LCST regime.

3.2.1 LCST regime. Spectroscopic ellipsometry illustrates that PNIPAM undergoes an LCST thermotransition up to solvent compositions of approximately x_D = 0.1 (Fig. 1). Fig. 2 and 3 demonstrate concordant behaviour, presenting the polymer volume fraction (VF) as a function of orthogonal distance from the substrate. PT-MCMC derived spread of the model, SLD and VF profiles are presented in the ESI, Fig. S3.3.† Initially, in D_2O (x_D = 0) and at 20 °C (Fig. 2), the PNIPAM brush is in its relatively most swollen state, with a broad low polymer VF inner region. Upon increasing the temperature to 27.5 °C and subsequently 32.5 °C, the brush undergoes a collapse before eventually entering its relatively most

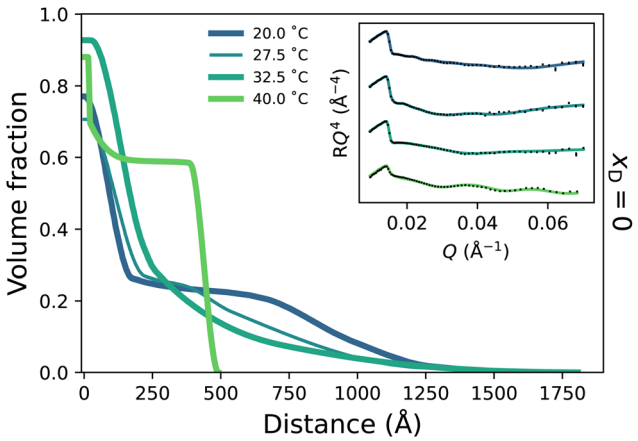

Fig. 2 Polymer volume fraction profiles of a PNIPAM brush as a function of temperature in D_2O. Thicker curves represent the VF profiles corresponding to the most swollen, partially collapsed and most collapsed structures. Inset presents corresponding reflectivity and models.

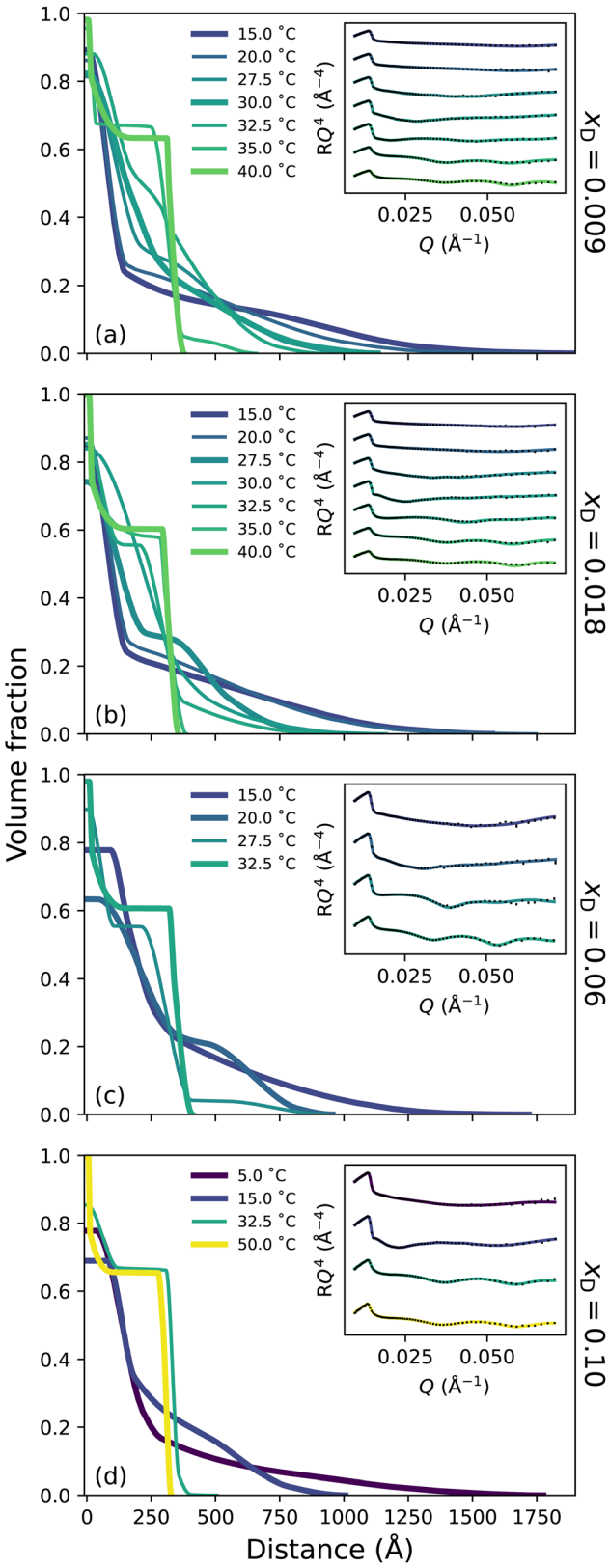

Fig. 3 Polymer volume fraction profiles of a PNIPAM brush as a function of temperature in (a) x_D = 0.009, (b) 0.018, (c) 0.06 and (d) 0.10. Thicker curves represent the VF profiles corresponding to the most swollen, partially collapsed and most collapsed structures.

 This journal is © The Royal Society of Chemistry 2023

Open Access Article. Published on 10 Mart 2023. Downloaded on 9.09.2024 20:37:54.
This article is licensed under a Creative Commons Attribution-NonCommercial 3.0 Unported Licence.

collapsed state at 40 °C, being 'slab-like' with a well-defined inner region. This behaviour aligns with our previously reported studies.[3,46,50]

In the presence of binary DMSO–water mixtures, the brush structure as a function of temperature is altered (Fig. 3). At x_D = 0.009, increasing the temperature leads to a monotonic decrease in the extension of the diffuse tail of the brush as well as an increase in the polymer VF corresponding to the inner region. In the most collapsed cases (*i.e.*, high temperatures), a proximal layer of negligible size is also observed. These features are also discerned at x_D = 0.018, 0.06 and 0.10, where the slab-like nature of the brush prevails as the onset of collapse occurs at lower temperatures with increasing x_D. The well-known bottom-up collapse that PNIPAM brushes exhibit in aqueous electrolytes is also observed here in binary DMSO–water mixtures, where the polymer VF of the inner region increases with increasing temperature whilst the diffuse tail remains low.[3,8,56] Corresponding brush thicknesses extracted from the VF profile first moment are presented in Fig. S3.1a,† aligning with ellipsometry measurements (Fig. 1).

The presence of small concentrations of DMSO is known to decrease the thermotransition temperature and swelling of PNIPAM; however, the impact of solvent composition on the structural behaviour of a PNIPAM/polymer brush has not been previously investigated. Here we observe a non-linear, monotonic decrease in LCST up to x_D = 0.10, which is most evident in Fig. S2.1.† In the binary solvent mixtures examined, there exists a competition between DMSO and PNIPAM for water molecules. Overall, DMSO–water hydrogen-bonds are the strongest of any solvent–solute interaction, and the (hydrophobic) hydration of the DMSO methyl group is more enthalpically favourable than (hydrophobic) methyl–methyl association.[14] The resultant formation of 1DMSO : $2H_2O$ clusters promotes the dehydration of PNIPAM as the number of water molecules available to solvate the PNIPAM chains decreases with x_D. Specifically, the addition of DMSO promotes the cooperative relaxation of the hydrogen-bond network,[28] and retards the reorientation of water molecules.[20] In this instance, the NR polymer VF profiles demonstrate that the addition of DMSO to the system results in a shift in polymer thermotransition to lower temperatures due to the formation of DMSO–water clusters, whilst the structure of the brush remains analogous to that of pure water at relative temperatures, including the persistence of the bottom-up collapse. Despite the formation of DMSO–water hydrogen-bonds, neutron scattering and molecular dynamics simulations demonstrate that at these low x_D the local (first coordination shell) tetrahedral structure of water is preserved.[26,30,57] However, the formation of the DMSO–water aggregates disrupt the long-range coordination of water, as the addition of DMSO disrupts the tetrahedral structure of water beyond the second coordination shell with increasing x_D. This change in water–water coordination is supported by FTIR spectroscopy in Fig. S1.2,† which was employed to monitor changes in the DMSO S═O stretch and CH_3 rocking with increasing x_D. Here only slight changes in the amount of hydrogen-bonded DMSO occur over this x_D range.

3.2.2 Cononsolvency regime. Prior investigations into the swelling behaviour of untethered PNIPAM and PNIPAM gels in DMSO–water mixtures have unveiled a large cononsolvency region in the presence of significant mole fractions of both solvents.[11,38,42] Tethered polymers, however, have proven to be a unique exemplar case as surface characterisation techniques permit measurements in 'poor' solvent conditions. Despite this, the structure of polymer brushes in this cononsolvency regime has not yet been probed. The range of solvent compositions that exhibit cononsolvency behaviour is quite broad and has previously been attributed to strong, favourable hydrogen-bonds formed between DMSO and water molecules.[11,38] Interestingly, we observed an apparent cononsolvency effect at x_D = 0.20 but not around equal mole fractions of DMSO and water at x_D = 0.50 and 0.60. Fig. 4 presents the polymer VF profiles of a PNIPAM brush in x_D = 0.20, 0.50 and 0.60 at select temperatures, revealing details of the subtle changes in brush structure across this region.

Broadly, the set of polymer VF profiles at x_D = 0.20, 0.50 and 0.60 become more solvated with increasing x_D, which is in concert with a slight increase in the diffuse nature of the polymer brush periphery. Specifically, at x_D = 0.20 (Fig. 4a) no thermoresponse is observed across the probed temperature range: the brush remains slab-like at all temperatures explored and no change in the internal structure of the brush is observed. This is a result of the cononsolvency behaviour exhibited at intermediate molarity DMSO–water mixtures with PNIPAM.[11,38] However, at x_D = 0.50 (Fig. 4b) a visible change in polymer brush conformation is observed with increasing temperature: at all temperatures, the area proximal to the substrate appears to be slightly more solvated than at x_D = 0.20, which is accompanied by a significantly higher roughness between the proximal layer and the inner region. Moreover, as temperature increases, the inner region of the brush decreases slightly in polymer VF whilst also increasing in thickness. At x_D = 0.60 (Fig. 4c), an interesting behaviour is observed; the brush undergoes no significant change in conformation up until exposure to 50 °C. At all temperatures, the brush periphery is slightly diffuse, but a distinct inner slab-like region remains. However, at 50 °C, the VF of polymer at this inner region decreases, indicating that the brush is more solvated. Interestingly, whilst the brush structure is observed to change, the NR derived brush thickness (Fig. S3.1b†) exhibits negligible changes across these temperatures. We hypothesise that this modulation in brush structure at 50 °C heralds the onset of UCST behaviour.

Previous investigations probing the behaviour of PNIPAM in the DMSO–water cononsolvency regime employed ungrafted PNIPAM, whereby subtle details in polymer swelling and structure are lost. However, one study by Espinosa-Marzal *et al.* probed the behaviour of dextran brushes using an extended surface force apparatus, noting a decrease in swelling with increasing x_D up to x_D = 0.5, followed by a subsequent increase.[58] Here, for the first time, we investigate tethered PNIPAM brushes with leading surface characterisation techniques which suggest that the cononsolvency region is nar-

Open Access Article. Published on 10 Mart 2023. Downloaded on 9.09.2024 20:37:54.
This article is licensed under a Creative Commons Attribution-NonCommercial 3.0 Unported Licence.

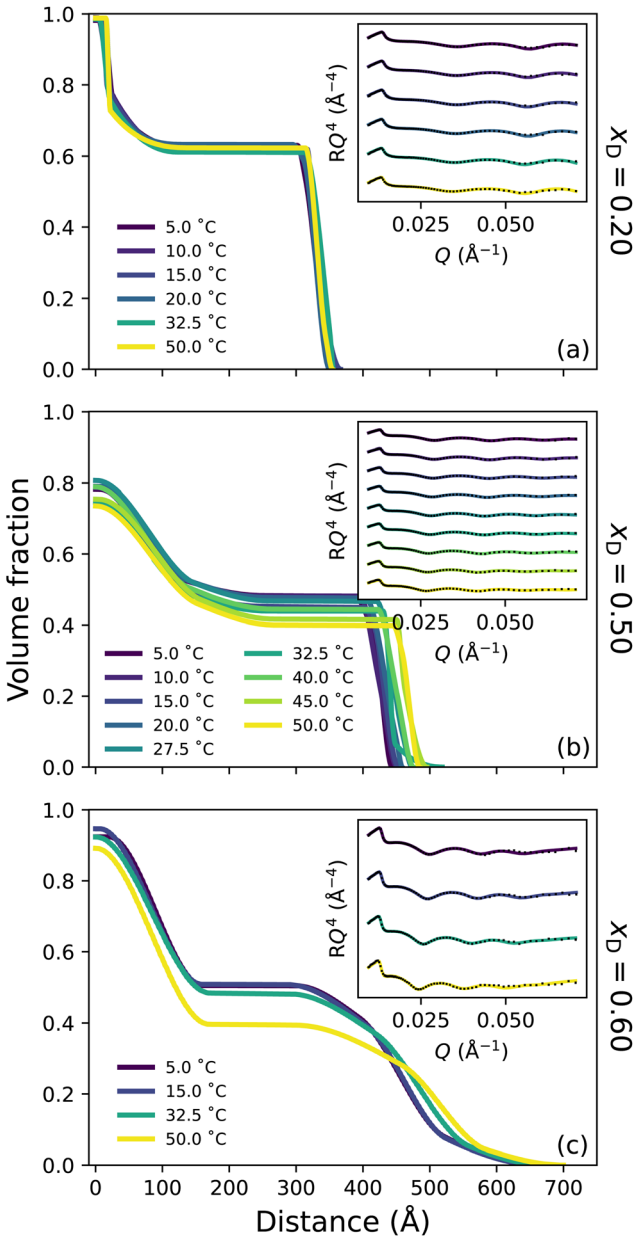

Fig. 4 Polymer volume fraction profiles of a PNIPAM brush derived by neutron reflectometry in various solvent compositions of increasing x_D as a function of temperature: (a) x_D = 0.20, (b) 0.50 and (c) 0.60. Inset presents corresponding reflectivity and models.

rower than previously proposed;[11,38] both ellipsometry and NR indicate reentrant swelling occurs after x_D = 0.20. In particular, in these intermediate solvent compositions, the brush appears to be more solvated at all temperatures relative to the brush in lower x_D at higher temperatures. These NR derived polymer VF profiles are concordant with the ellipsometry data presented in Fig. 1.

Here, the chaotropic nature of DMSO is evident and has a detrimental influence on the tetrahedral structure of water, which decreases up to x_D = 0.60.[24] A previous study by Ishidao *et al.* investigated the influence of binary DMSO–water solvents on the swelling of PNIPAM gels.[42] When comparing the solvent composition inside the gel relative to the bulk, the authors deduced that the concentrations were approximately equal across the entire range. However, Raman spectroscopy studies on ungrafted PNIPAM in DMSO–water mixtures by Yamauchi *et al.* propose that upon collapse, DMSO is excluded from the polymer-rich phase throughout the cononsolvency regime due to the prevailing DMSO–water hydrogen-bonds.[11] This aligns with all polymer VF profiles presented here, which illustrate a high VF of polymer in the proximal layer upon collapse. We hypothesise that for the brush regime, the shape and size of the solvent clusters play an integral role in the solvation of a polymer brush and that it is naive to conclude that only a single type of solvent cluster will exist at a given x_D.[13] As such, at approximately equimolar concentrations 1DMSO : 1H_2O aggregates prevail.[14,19,23,31] FTIR spectroscopy (Fig. S1.2†) suggests that the fraction of non-self-associated DMSO (and self-associated DMSO) systemically increases with x_D. These small clusters are capable of entering the brush and interacting with PNIPAM *via* both hydrogen-bonds and dipole–dipole interactions. We suggest that these small clusters are the driving force behind the slight increase in solvation (reentrant swelling) of PNIPAM across intermediate x_D. We also propose that this may be the origin of the slightly lower polymer VF in the proximal layer for x_D = 0.50 relative to both x_D = 0.20 and x_D = 0.60.

3.2.3 DMSO-rich regime. In DMSO-rich solvent compositions, ungrafted PNIPAM is known to undergo a UCST thermotransition; a collapsed to swollen transition with increasing temperature.[11,38] The NR derived polymer VF profiles in Fig. 5a and b demonstrate this behaviour, illustrating a clear modulation in structure with increasing temperature. Specifically, at x_D = 0.70 and 5 °C (Fig. 5a) the brush is in its relatively most collapsed conformation, yet the brush exhibits a more diffuse tail region relative to the lower x_D conditions previously mentioned. No significant changes in brush conformation are observed until 32.5 °C, where solvation in the inner brush region increases slightly. Upon further heating to 50 °C, the brush has undergone a UCST thermotransition and exhibits its relatively most swollen conformation. Analogous behaviour is also observed for the brush in x_D = 0.8 (Fig. 5b), with the thermotransition onset occurring at slightly lower temperatures. Corresponding swelling ratios as a function of temperature and solvent composition are presented in Fig. S3.1.† The swollen brush regime for all UCST behaviour observed is distinctly different from that observed for LCST behaviour. The 'swollen' polymer VF profiles in Fig. 5a and b present a much more diffuse brush than those presented in Fig. 3.

In this DMSO-rich regime, the origin of the UCST behaviour exhibited by PNIPAM lies in dipole–dipole interactions, as non-site-specific PNIPAM–DMSO and DMSO–DMSO interactions begin to prevail over the aforementioned site-specific interactions.[28,38] This percolating hydrophobic network results in significant disruption of the DMSO–water hydrogen-bond network into smaller aggregates, accelerating the reorientation

 This journal is © The Royal Society of Chemistry 2023

Open Access Article. Published on 10 Mart 2023. Downloaded on 9.09.2024 20:37:54.
This article is licensed under a Creative Commons Attribution-NonCommercial 3.0 Unported Licence.

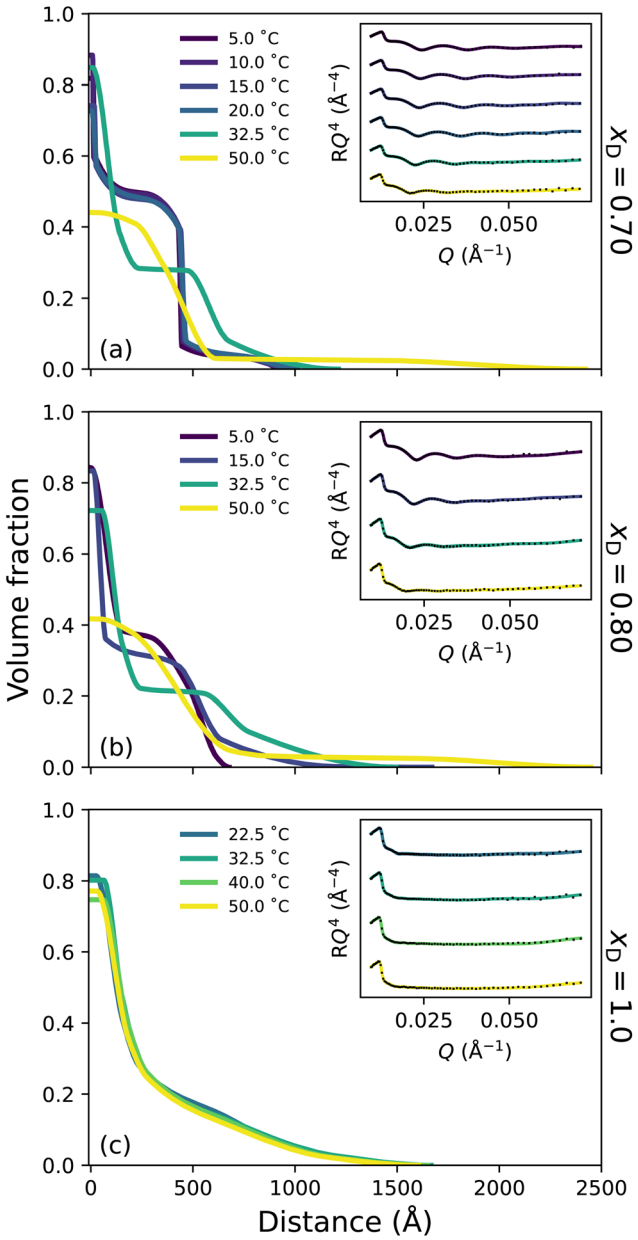

Fig. 5 Polymer volume fraction profiles of a PNIPAM brush derived by neutron reflectometry in various solvent compositions of increasing as a function of temperature: (a) x_D = 0.70, (b) 0.80 and (c) 1.0 (pure DMSO). Inset presents corresponding reflectivity and models.

of water molecules.[20,28] Specifically, below the UCST, solvent molecules are present in aggregates that are too large to solvate the brush. However, increasing temperature above the UCST results in an increase in system entropy, rupturing hydrogen-bond aggregates and allowing polymer solvation. Here PNIPAM solvation is dominated by non-site-specific dipole–dipole interactions and accompanied by site-specific hydrogen-bond interactions. The increased diffuse structure in these DMSO-rich regimes could be attributed to the periphery solvation of the PNIPAM brush by larger DMSO–water aggregates.

Fig. 5c presents the polymer VF profile corresponding to PNIPAM in DMSO (x_D = 1), a 'good' solvent for PNIPAM.[38,54] In this particular regime, DMSO–PNIPAM interactions are stronger than any solvent interaction. Consequently, the PNIPAM brush is swollen and diffuse at all probed temperatures, exhibiting no thermotransition which aligns with previous investigations on ungrafted PNIPAM.[11,38] No significant changes in brush structure are observed for the pure DMSO case.

4 Conclusion

Techniques typically restricted to aqueous solutions were employed in this study to probe the changes in thermoresponse and structure of a PNIPAM brush in binary DMSO–water mixtures. Here we monitor changes in brush behaviour with both spectroscopic ellipsometry and neutron reflectometry to probe changes in solvent structure across aqueous DMSO mixtures. The use of tethered polymers in this novel study was of particular significance as the behaviour of PNIPAM could be thoroughly explored over the entire solvent composition space. FTIR spectroscopy was also employed to monitor changes in the DMSO S═O stretch and CH_3 rocking as a function of x_D. Both spectroscopic ellipsometry and NR unmasked changes in brush swelling, revealing LCST behaviour up to approximately x_D = 0.10; decreasing in a non-linear fashion with increasing x_D. Here the structure of the brush was analogous to that in pure water (x_D = 0), including the persistence of the 'bottom-up collapse'. At slightly higher concentrations of DMSO ($x_D \approx 0.20$), binary solvents of DMSO and water impart cononsolvency effects, whereby the structure of the brush was observed to be slab-like. At higher DMSO concentrations in the cononsolvency regime (up to x_D = 0.50), reentrant swelling was observed with increasing x_D, where minor changes in brush swelling are noted with increasing temperature. Previous studies on ungrafted PNIPAM/polymer have not reported reentrant swelling. In the DMSO-rich regime, PNIPAM exhibits a UCST whereby hydrogen-bonds between DMSO–water aggregates are ruptured with increasing temperature, permitting the solvation of the PNIPAM brush. Relative to a swollen brush in a low x_D, the swollen brush in high x_D exhibits a significantly more diffuse periphery. Previous studies on PNIPAM gels have not noted UCST behaviour. Upon exposing the brush to pure DMSO (x_D = 1.0), no thermoresponse was observed for the experimentally probed temperatures and the brush is swollen and diffuse at all temperatures; DMSO is a 'good' solvent for PNIPAM. This study presents methodologies to examine the thermoresponse behaviour and conformation of polymer brushes in complex, non-aqueous environments; probing conformations that are not observable by other techniques employed with ungrafted polymer. As such, this study establishes a precedent for the future characterisation of both polymer gels and brushes in complex media for future technologies.

Open Access Article. Published on 10 Mart 2023. Downloaded on 9.09.2024 20:37:54.
This article is licensed under a Creative Commons Attribution-NonCommercial 3.0 Unported Licence.

Author contributions

Hayden Robertson: Conceptualisation, methodology, investigation, formal analysis, software, data curation, writing – original draft, visualisation, writing – review & editing, funding acquisition. Andrew R. J. Nelson: Methodology, software, writing – review & editing, supervision, funding acquisition. Stuart W. Prescott: Investigation, software, supervision, funding acquisition. Grant B. Webber: Conceptualisation, project administration, resources, writing – review & editing, supervision, funding acquisition. Erica J. Wanless: Conceptualisation, project administration, resources, writing – review & editing, supervision, funding acquisition.

Conflicts of interest

There are no conflicts to declare.

Acknowledgements

This research was supported by the Australian Research Council (DP190100788) and ANSTO (P8553). HR thanks the Australian Government for providing a Research Training Program Scholarships and AINSE Ltd for a Post Graduate Research Award. Dr Edwin Johnson, Dr Isaac Gresham and Dr Kasimir Gregory are thanked for their assistance with neutron reflectometry experiments.

References

1 M. A. Cohen Stuart, W. T. Huck, J. Genzer, M. Müller, C. Ober, M. Stamm, G. B. Sukhorukov, I. Szleifer, V. V. Tsukruk, M. Urban, F. Winnik, S. Zauscher, I. Luzinov and S. Minko, *Nat. Mater.*, 2010, **9**, 101–113.
2 H. Robertson, E. C. Johnson, I. J. Gresham, S. W. Prescott, A. Nelson, E. J. Wanless and G. B. Webber, *J. Colloid Interface Sci.*, 2021, **586**, 292–304.
3 H. Robertson, J. D. Willott, K. P. Gregory, E. C. Johnson, I. J. Gresham, A. R. J. Nelson, V. S. J. Craig, S. W. Prescott, R. Chapman, G. B. Webber and E. J. Wanless, *J. Colloid Interface Sci.*, 2023, **634**, 983–994.
4 M. Concilio, V. P. Beyer and C. R. Becer, *Polym. Chem.*, 2022, **13**, 6423–6474.
5 M. A. Ward and T. K. Georgiou, *Polymers*, 2011, **3**, 1215–1242.
6 D. Roy, W. L. Brooks and B. S. Sumerlin, *Chem. Soc. Rev.*, 2013, **42**, 7214–7243.
7 S. Peng and B. Bhushan, *RSC Adv.*, 2012, **2**, 8557–8578.
8 H. Schild, *Prog. Polym. Sci.*, 1992, **17**, 163–249.
9 Z. S. Klemenkova and E. G. Kononova, *J. Solution Chem.*, 2015, **44**, 280–292.
10 A. Halperin, M. Kröger and F. M. Winnik, *Angew. Chem., Int. Ed.*, 2015, **54**, 15342–15367.
11 H. Yamauchi and Y. Maeda, *J. Phys. Chem. B*, 2007, **111**, 12964–12968.
12 K. Noack, J. Kiefer and A. Leipertz, *ChemPhysChem*, 2010, **11**, 630–637.
13 A. Bertoluzza, S. Bonora, M. A. Battaglia and P. Monti, *J. Raman Spectrosc.*, 1979, **8**, 231–235.
14 Q. Zhang, X. Zhang and D. X. Zhao, *J. Mol. Liq.*, 2009, **145**, 67–81.
15 J. E. Lovelock and M. W. H. Bishop, *Nature*, 1959, **183**, 1394–1395.
16 Y. J. Zheng and R. L. Ornstein, *J. Am. Chem. Soc.*, 1996, **118**, 4175–4180.
17 T. J. Anchordoguy, C. A. Cecchini, J. H. Crowe and L. M. Crowe, *Cryobiology*, 1991, **28**, 467–473.
18 G. M. Sando, K. Dahl and J. C. Owrutsky, *J. Phys. Chem. B*, 2007, **111**, 4901–4909.
19 V. M. Wallace, N. R. Dhumal, F. M. Zehentbauer, H. J. Kim and J. Kiefer, *J. Phys. Chem. B*, 2015, **119**, 14780–14789.
20 X. Zhang, Z. Wang, Z. Chen, H. Li, L. Zhang, J. Ye, Q. Zhang and W. Zhuang, *J. Phys. Chem. B*, 2020, **124**, 1806–1816.
21 D. H. Rasmussen and A. P. Mackenzie, *Nature*, 1968, **220**, 1315–1317.
22 J. M. G. Cowie and P. M. Toporowski, *Can. J. Chem.*, 1961, **39**, 2240–2243.
23 J. Catalán, C. Díaz and F. García-Blanco, *J. Org. Chem.*, 2001, **66**, 5846–5852.
24 C. Nieto-Draghi, J. B. Ávalos and B. Rousseau, *J. Chem. Phys.*, 2003, **119**, 4782–4789.
25 L. J. Yang, X. Q. Yang, K. M. Huang, G. Z. Jia and H. Shang, *Int. J. Mol. Sci.*, 2009, **10**, 1261–1270.
26 A. K. Soper and A. Luzar, *J. Phys. Chem.*, 1996, **100**, 1357–1367.
27 M. I. Sastry and S. Singh, *J. Raman Spectrosc.*, 1984, **15**, 80–85.
28 Z. Lu, E. Manias, M. Lanagan and D. Macdonald, *ECS Trans.*, 2010, **28**, 11–21.
29 J. T. Cabral, A. Luzar, J. Teixeira and M.-C. Bellissent-Funel, *J. Chem. Phys.*, 2000, **113**, 8736–8745.
30 S. E. McLain, A. K. Soper and A. Luzar, *J. Chem. Phys.*, 2007, **127**, 174515.
31 B. Kirchner and M. Reiher, *J. Am. Chem. Soc.*, 2002, **124**, 6206–6215.
32 A. D. Fortes, J. Ponsonby, O. Kirichek and V. García-Sakai, *Acta Crystallogr., Sect. B: Struct. Sci., Cryst. Eng. Mater.*, 2020, **76**, 733–748.
33 I. A. Borin, *J. Chem. Phys.*, 1999, **110**, 6412–6420.
34 L. Liu, T. Wang, C. Liu, K. Lin, G. Liu and G. Zhang, *J. Phys. Chem. B*, 2013, **117**, 10936–10943.
35 D. Mukherji, C. M. Marques and K. Kremer, *Nat. Commun.*, 2014, **5**, 1–6.
36 I. Bischofberger, D. C. Calzolari, P. De Los Rios, I. Jelezarov and V. Trappe, *Sci. Rep.*, 2014, **4**, 1–7.
37 T. Wang, G. Liu, G. Zhang and V. S. Craig, *Langmuir*, 2012, **28**, 1893–1899.
38 R. O. Costa and R. F. Freitas, *Polymer*, 2002, **43**, 5879–5885.

 This journal is © The Royal Society of Chemistry 2023

Open Access Article. Published on 10 Mart 2023. Downloaded on 9.09.2024 20:37:54.
This article is licensed under a Creative Commons Attribution-NonCommercial 3.0 Unported Licence.

39 S. Katayama, Y. Hirokawa and T. Tanaka, *Macromolecules*, 1984, **17**, 2641–2643.
40 K. Mukae, M. Sakurai, S. Sawamura, K. Makino, S. W. Kim, I. Ueda and K. Shirahama, *Colloid Polym. Sci.*, 1994, **272**, 655–663.
41 G. Liu and G. Zhang, *Langmuir*, 2005, **21**, 2086–2090.
42 T. Ishidao, Y. Hashimoto, Y. Iwai and Y. Arai, *Colloid Polym. Sci.*, 1994, **272**, 1313–1316.
43 M. Karg, S. Prévost, A. Brandt, D. Wallacher, R. von Klitzing and T. Hellweg, *Intelligent Hydrogels*, Cham, 2013, pp. 63–76.
44 B. A. Humphreys, E. J. Wanless and G. B. Webber, *J. Colloid Interface Sci.*, 2018, **516**, 153–161.
45 B. A. Humphreys, J. D. Willott, T. J. Murdoch, G. B. Webber and E. J. Wanless, *Phys. Chem. Chem. Phys.*, 2016, **18**, 6037–6046.
46 T. J. Murdoch, B. A. Humphreys, J. D. Willott, K. P. Gregory, S. W. Prescott, A. Nelson, E. J. Wanless and G. B. Webber, *Macromolecules*, 2016, **49**, 6050–6060.
47 H. Robertson, I. J. Gresham, S. W. Prescott, G. B. Webber, E. J. Wanless and A. Nelson, *SoftwareX*, 2022, **20**, 101225.
48 H. Robertson, A. R. J. Nelson, S. W. Prescott, G. B. Webber and E. J. Wanless, 2022, DOI: **10.5281/zenodo.7359325**, ESI† for "Cosolvent effects on the structure and thermoresponse of a PNIPAM brush".
49 M. James, A. Nelson, S. A. Holt, T. Saerbeck, W. A. Hamilton and F. Klose, *Nucl. Instrum. Methods Phys. Res., Sect. A*, 2011, **632**, 112–123.
50 I. J. Gresham, T. J. Murdoch, E. C. Johnson, H. Robertson, G. B. Webber, E. J. Wanless, S. W. Prescott and A. R. J. Nelson, *J. Appl. Crystallogr.*, 2021, **54**, 739–750.
51 I. J. Gresham, B. A. Humphreys, J. D. Willott, E. C. Johnson, T. J. Murdoch, G. B. Webber, E. J. Wanless, A. R. Nelson and S. W. Prescott, *Macromolecules*, 2021, **54**, 2541–2550.
52 A. R. J. Nelson and S. W. Prescott, *J. Appl. Crystallogr.*, 2019, **52**, 193–200.
53 J.-F. F. Lutz, Ö. Akdemir and A. Hoth, *J. Am. Chem. Soc.*, 2006, **128**, 13046–13047.
54 N. Ishida and S. Biggs, *Macromolecules*, 2010, **43**, 7269–7276.
55 A. M. Jonas, K. Glinel, R. Oren, B. Nysten and W. T. S. Huck, *Macromolecules*, 2007, **40**, 4403–4405.
56 X. Laloyaux, B. Mathy, B. Nysten and A. M. Jonas, *Langmuir*, 2010, **26**, 838–847.
57 A. K. Soper and A. Luzar, *J. Chem. Phys.*, 1992, **97**, 1320–1331.
58 R. M. Espinosa-Marzal, P. C. Nalam, S. Bolisetty and N. D. Spencer, *Soft Matter*, 2013, **9**, 4045–4057.